NASA Technical Memorandum 101701

Effects of Wing Sweep on In-Flight Boundary-Layer Transition for a Laminar Flow Wing at Mach Numbers From 0.60 to 0.79

Bianca Trujillo Anderson and Robert R. Meyer, Jr.

July 1990

NASA

National Aeronautics and Space Administration

NASA Technical Memorandum 101701

Effects of Wing Sweep on In-Flight Boundary-Layer Transition for a Laminar Flow Wing at Mach Numbers From 0.60 to 0.79

Bianca Trujillo Anderson and Robert R. Meyer, Jr.
Ames Research Center, Dryden Flight Research Facility, Edwards, California

1990

National Aeronautics and
Space Administration
Ames Research Center
Dryden Flight Research Facility
Edwards, California 93523-0273

CONTENTS

LIST OF FIGURES

SUMMARY

The variable-sweep transition flight experiment (VSTFE) was conducted on an F-14A variable-sweep wing fighter to examine the effect of wing sweep on natural boundary-layer transition. Nearly full span upper surface gloves, extending to 60-percent chord, were attached to the F-14 aircraft's wings. This report presents the results of the glove 2 flight tests. Glove 2 had an airfoil shape designed for natural laminar flow at a wing sweep of 20°. Sample pressure distributions and transition locations are presented with the complete results tabulated in a database. Data were obtained at wing sweeps of 15, 20, 25, 30, and 35°, at Mach numbers ranging from 0.60 to 0.79, and at altitudes ranging from 10,000 to 35,000 ft. Results show that a substantial amount of laminar flow was maintained at all the wing sweeps evaluated. The maximum transition Reynolds number obtained was 18.6×10^6 at 15° of wing sweep, Mach 0.75, and at an altitude of 10,000 ft.

INTRODUCTION

Maintaining a laminar boundary layer over a large portion of an aircraft wing and empennage can reduce drag appreciably and benefit transports of all sizes (refs. 1–5). Laminar flow can be achieved through active or passive means. The active method uses suction through slots or holes in the wing surface to maintain laminar flow up to, potentially, 100 percent of the wing chord at very high Reynolds numbers. The passive method requires a smooth surface and proper shaping of the wing to obtain a pressure distribution with favorable gradients to maintain laminar flow.

Determining the transition location at conditions representative of transport aircraft has been limited mostly to full-scale flight testing. The required Reynolds numbers, model size, and low turbulence levels limited the use of wind tunnels. Also, accurate predictions of the boundary-layer transition location are difficult to obtain because boundary-layer stability codes are still being developed and verified.

Maintaining laminar flow through passive means was thought to be limited to low sweep angles ($\Lambda \leq 20°$). High sweep angles and high Reynolds numbers increase the possibility of early boundary-layer transition caused by crossflow disturbances and leading-edge contamination. Crossflow disturbances travel from inboard to outboard on the wing and are a result of wing sweep. Leading-edge contamination is turbulent flow which starts from the fuselage inboard or wing leading edge and travels outboard, along the leading-edge attachment line, precluding laminar flow on the wing.

One earlier flight test yielding encouraging results was a joint National Aeronautics and Space Administration (NASA) Ames Research Center Dryden Flight Research Facility (Ames-Dryden) and NASA Langley Research Center experiment flown on the variable-sweep F-111 transonic aircraft technology (TACT) aircraft. The TACT natural laminar flow (NLF) experiment (refs. 1, 6, 7, and 8) provided the first definitive flight results showing the effects of wing sweep on boundary-layer transition. The NLF experiment used a full chord glove with a super-critical NLF airfoil shape. The right wing panel of the F-111 TACT aircraft was partially covered with a glove which had a span of approximately 6 ft and a chord of 10 ft. The glove was designed to provide a favorable pressure gradient to about 70-percent chord at a wing sweep of 10°.

Although limited, the F-111 TACT aircraft NLF results indicated that the adverse effect of leading-edge sweep was less than expected in earlier assumptions (ref. 6). Data from the F-111 TACT aircraft NLF flight experiment have also been used to enhance boundary-layer stability prediction methods (ref. 8).

Based on the favorable F-111 TACT aircraft NLF results, the variable-sweep transition flight experiment (VSTFE), using an F-14A aircraft, was initiated by NASA Langley and NASA Ames-Dryden. The wing panels of the F-14 variable-sweep aircraft were modified with nearly full span, partial chord gloves that had smooth surfaces and a substantial amount of favorable pressure gradient, suitable for NLF.

The primary objectives of the F-14 aircraft VSTFE were:

1. Determine the effects of wing sweep as a function of pressure distribution, Reynolds number, Mach number, and angle of attack on boundary-layer transition at flight conditions representative of transport aircraft.
2. Establish a boundary-layer transition database for laminar flow wing design and for evaluation of analytical techniques used to predict the transition location.
3. Determine transition location using two different measurement techniques and a flow visualization technique, and compare the transition data obtained from each technique.

Two different gloves were flight-tested in the VSTFE: glove 1, a smoothing of the basic F-14 wing, and glove 2, designed to provide favorable pressure distributions for natural laminar flow at Mach (M) 0.70 (refs. 9 and 10). Reports documenting the wing glove designs, flight test techniques and glove 1 results are in references 10 through 15.

This report documents and analyzes data from glove 2 of the VSTFE. Data were obtained at Mach numbers from 0.60 to 0.79, altitudes ranging from 10,000 to 35,000 ft, and wing sweeps from 15 to 35°. This report does not address objective 3, which has been reported in reference 14. A complete tabulation of the surface pressure distribution, boundary-layer transition, and boundary-layer rake data is listed in this report.

NOMENCLATURE

Terms in parentheses are computer-generated terms used in the microfiche supplement.

AG	nondimensional chordwise location of the onset of the adverse pressure gradient
BL	butt line location, in.
c	chord length, in.
C_p (Cp)	coefficient of pressure, $(p - p_s)/\bar{q}$
FM	frequency modulation
hp	altitude, ft
M	free-stream Mach number
NACA	National Advisory Committee for Aeronautics
NASA	National Aeronautics and Space Administration
NLF	natural laminar flow
p	local static pressure, lb/ft^2
p_s	free-stream static pressure, lb/ft^2
p_t	total pressure, lb/ft^2
$\bar{q}$ (QBAR)	dynamic pressure, $0.70 p_s$ Mach^2, lb/ft^2
Re_T (ReT)	transition Reynolds number, Rnpu $\times x_T/12.00$
Rnpu	Reynolds number per unit foot, $\rho_\infty U_\infty/\mu_\infty$, 1/ft
TACT	transonic aircraft technology
U	local velocity, ft/sec
U_{max}	average maximum velocity at rake location, ft/sec

U/Umax	U/U_{max}, computer-generated term used in microfiche supplement
VSTFE	variable-sweep transition flight experiment
x	distance from glove leading edge, in.
(x/c)T	$(x/c)_T$, computer-generated term used in microfiche supplement
Y	boundary-layer rake probe height, in.
y	distance from airfoil centerline
α	angle of attack, deg
β	angle of sideslip, deg
δ	boundary-layer height, in.
$\delta*$	displacement thickness, $\int_0^\delta (1 - \rho U/\rho_{max} U_{max})\, dy$, in.
Λ	leading-edge wing sweep, deg
Λ_{eq}	equivalent wing sweep $(\Lambda - \beta)$, deg
θ	momentum thickness, $\int_0^\delta (1 - \rho U/\rho_{max} U_{max})\, dy$, in.
ρ	density, slug/ft^3
ρ_{max}	density outside of the boundary layer
μ	absolute viscosity, slug/ft-sec

Subscripts

T	transition location
∞	free stream

DESCRIPTION OF THE AIRCRAFT CONFIGURATION

Aircraft Description

The F-14A aircraft is a two place, variable-sweep wing fighter aircraft powered by two TF30-P414 engines. The wings can be swept from 20 to 68°. The NLF gloves were attached to the upper surface of each wing. Figure 1 shows the F-14A aircraft with glove 1 on the left wing and glove 2 on the right wing. With the gloves installed, the wing-sweep capability was restricted to a range of 20 to 35° and the flaps and slats were locked in a retracted position.

Glove 2

Glove 2 provided an NLF airfoil shape designed to achieve an extensive favorable pressure gradient over the upper surface. Although glove 2 was initially designed for 20° of sweep and M = 0.70, it also provided a variety of pressure distributions over a broad range of Mach numbers for which transition data could be obtained. Therefore, glove 2 had no specific design condition except for 20° of sweep. Table 1 presents glove 2 airfoil coordinates at four span stations.

As figure 2 shows, the glove, which was constructed of foam and fiberglass, wrapped around the wing leading edge and extended back to the spoiler hinge line on the upper surface (~60-percent chord). The glove covered

the majority of the wing span as figure 1 shows. The details of glove construction techniques are discussed in references 16 and 17.

The waviness of the glove surface was inspected and documented. Figure 3(a) presents surface waviness measurements for four wing stations on glove 2. The measurements were obtained with a mechanical deflection dial gauge having support feet which were 2 in. apart (fig. 3(b)). The dial gauge was attached to a wheel from which the distance along the glove surface could be determined. The outputs from both the dial gauge and the wheel were automatically plotted when the unit was manually moved across the surface. The waves measured on the glove were within 0.002-in. amplitude for 2-in. distance, the criterion specified for glove construction.

INSTRUMENTATION

Figure 4 shows the glove 2 instrumentation layout which consisted of:

1. Four rows of flush static pressure orifices,
2. fifteen hot-film sensors with variable location of the ratio from leading edge to local chord length (x/c), and
3. two boundary-layer rakes.

In addition, liquid crystals were used for flow visualization of boundary-layer transition on the F-14A gloves (refs. 14 and 15). The glove instrumentation systems were located in three test sections: inboard, between butt line location (BL) stations 160 and 204; middle, between BL stations 204 and 264; and outboard, between BL stations 264 and 324. A fourth row of flush static orifices were inboard of the test sections at BL station 140.

The following instrumentation systems were installed on the aircraft at locations other than the wing glove:

1. A charge patch, on the left vertical tail,
2. an uplink guidance system, in the cockpit, and
3. a standard National Advisory Committee for Aeronautics (NACA) airdata noseboom.

All signals from the instruments were recorded onboard the aircraft, and most were downlinked to a ground station for real-time display and recording. Each instrumentation system previously mentioned is described in the following paragraphs.

Wing Pressure Instrumentation

Flush Static Pressure Orifices

Flush static pressure orifices were created by drilling through the glove foam and fiberglass to a cavity, 1-in. in diameter, created by a "target cup." The target cup was glued to the wing surface and buried in the glove as described in reference 17. Each orifice had an inside diameter of 0.03 in. The individual target cups were connected to a pressure transducer by 1/16-in.-inner diameter steel tubing. The maximum tube length was approximately 10 ft. Each orifice row consisted of 24 surface pressure orifices oriented parallel to the airflow for a wing sweep of 20°. Table 2 presents the details of each orifice row.

Boundary-Layer Rakes

Each boundary-layer rake was located at 0.55 x/c and consisted of 20 pitot pressure probes. To obtain more measurements in the boundary layer with a minimum of probe interference, the probes were mounted along a 5-in., slanted strut which was skewed 30° to the plane of the glove surface (fig. 5). With this type of rake orientation, the maximum probe distance from the glove surface was approximately 2.5 in. The rake probes were chamfered for less sensitivity to flow angularity. Each rake was aligned with the flow for a wing sweep of 20°. The pressures were measured by a pressure transducer. The maximum tube lengths were approximately 10 ft with a 1/16-in.-inner diameter. Table 3 presents the nominal boundary-layer rake probe heights.

Pressure Transducers

The pressures on the wing were measured by electronic scanning pressure modules. Each pressure module contained 32 differential pressure transducers. The transducer ranges were ± 5 lb/in^2 used to measure the glove static pressures, and ± 10 lb/in^2 used to measure the rake probe pressures. The lag in the pressure measurement system was estimated to be approximately one-tenth of a second. The pressure data was obtained at 7.4 samples/sec.

Hot-Film Anemometer System

The hot-film system used temperature compensated hot-film anemometers, which are described in references 14 and 18. The hot-film data were limited to a frequency response of 10 kHz by the frequency modulation (FM) tape recorder. The hot-film sensors (fig. 6) were mounted along a line oriented 30° inboard relative to each orifice row (fig. 4). This minimized the effects of flow disturbance from one sensor on another (flow is turbulent after each sensor). Each individual hot-film sensor was aligned with the flow at a wing sweep of 25°. Fifteen hot-film sensors were operational for each flight. The location of the operational hot-films varied from flight to flight (table 4).

Aircraft Instrumentation

The airdata system, a standard NACA/NASA airdata head, measured aircraft total and static pressures, angle of attack, and angle of sideslip. The total and static pressures were used to calculate parameters such as Mach number and dynamic pressure. Airspeed calibration data were obtained from a tower fly-by method and an acceleration-deceleration method (refs. 19 and 20). A complete description of a comparable airdata system is found in reference 21. The angle-of-attack and -sideslip flow direction vanes were mounted on the noseboom. Angle of attack was corrected for upwash and fuselage bending as described in reference 19.

Charge Patch

A charge patch detected the presence of ice particles or cirrus clouds. A detailed description of the charge patch can be found in references 15 and 22. For the data presented in this report, the charge patch indicated the absence of ice particles or cirrus clouds. Data correlating cirrus cloud encounters were not obtained for glove 2 because of the minimal number of cloud formations during the glove 2 flight tests.

Uplink Guidance System

The uplink is a flight trajectory guidance system that uses an analog cockpit display which indicates, in real time, deviations from the desired flight conditions. In the VSTFE, the uplink was used to obtain accurate flight conditions in a timely manner for each test point. The parameters used to guide the pilot were Mach number (M), angle of attack (α), angle of sideslip (β), and altitude (hp). The uplink guidance system is discussed in detail in reference 23.

Accuracy

The pressure ranges for the transducers were scaled for the desired flight conditions. The hot-film sensor signals were calibrated and were responsive to a frequency well above 10 kHz, which was the frequency response of the onboard FM tape recorder. The estimated error in the flight measurements were:

coefficient of pressure (C_p)	± 0.01
Mach number (M)	± 0.005
angle of attack (α)	$\pm 0.5°$
angle of sideslip (β)	$\pm 0.5°$
free-stream static pressure (p_s)	± 0.7 lb/ft^2
total pressure (p_t)	± 0.7 lb/ft^2
laminar to turbulent boundary-layer transition ($(x/c)_T$)	$\pm 0.025\, x/c$

While the absolute accuracies of angle of attack and sideslip are $\pm$ 0.5°, the repeatability of the test conditions was excellent, based on comparisons of pressure distributions between flights. This was because of the uplink guidance system and the repeatability of the angle-of-attack vane calibration.

FLIGHT TEST CONDITIONS AND PROCEDURES

Glove 2 was tested at leading-edge sweep angles varying from 15 to 35°. Transition data at 15° of sweep were obtained by using a 5°-nose left sideslip maneuver. The Reynolds number ranged from approximately 1×10^6 to 4×10^6/ft, which corresponds to a minimum and maximum chord Reynolds number of 5×10^6 and 34×10^6 respectively. Transition data were obtained at conditions listed in table 5.

The glove 2 flight test program was divided into two phases. The phase one flights cleared an operating envelope shown in figure 7. The maximum airspeed limit with the glove installed was 450 kn indicated airspeed or $M = 0.84$, whichever occurred first.

The laminar flow data flights, phase two, were conducted within the cleared envelope. Test conditions were selected to establish a database documenting the boundary-layer transition location as a function of angle of attack, Mach number, and Reynolds number (altitude). Maneuvers performed during the coarse- and fine-resolution survey flights consisted primarily of trim points, level turns, and pushovers. The level turns were used to obtain data at greater than 1-g trim angles of attack, particularly at low altitudes which have high dynamic pressures. The pushovers were used to obtain data at lower than 1-g trim angles of attack.

The majority of the glove 2 flights were conducted in the early morning, before temperatures got too high. The glove surface, which was painted black, had to be kept below 80°F to prevent damage to the glove. Early morning flights also helped avoid insects. Following each flight the glove was inspected for insect impacts, which were documented. The majority of insect impacts were forward of 10-percent chord and, with very few exceptions, were not large enough to cause transition at the test altitudes. Prior to each flight the glove was cleaned and necessary repairs were made to the glove instrumentation.

RESULTS AND DISCUSSION

Figures 8 to 20 present selected results showing trends in the transition data. The table of figures lists the flight conditions for these data. The microfiche supplement contains tabulated glove section pressure coefficients (table 6) and boundary-layer velocity profile data (table 7), along with a tabulation of transition location obtained from the hot-film sensors for each test point (table 8).

The glove 2 boundary-layer transition locations were determined primarily from hot-film sensors, along with limited results from the boundary-layer rakes. Based on the analysis of reference 14, the hot-film data were the most repeatable, compared to boundary-layer rake and liquid crystal data. Reference 14 contains a complete discussion on the techniques used to determine transition, the techniques used to interpret the transition data, and comparison of the results obtained from each technique.

Pressure Distributions

Figure 8 shows typical pressure distributions for the middle test section at trim angles of attack and at $M = 0.70$ and $M = 0.79$ for $\Lambda = 20°$. The most notable characteristic is the change in the pressure gradient $[dC_p/d(x/c)]$ and pressure distribution shape with Mach number. At $M = 0.70$ the pressure distribution has a moderately favorable pressure gradient $[dC_p/d(x/c) < 0]$ that becomes adverse $[dC_p/d(x/c) > 0]$ near 0.4 x/c for all the conditions shown, except at 35,000 ft and $\alpha = 3.0°$. At $M = 0.79$ the favorable pressure gradient is steeper and extends to at least 0.5 x/c, where a normal shock wave occurs.

One undesirable characteristic of the pressure distribution at $M = 0.70$ was the formation of an adverse pressure gradient between 0.06 and 0.2 x/c at trim angles of attack ($\alpha = 2.5°$ and above) at the highest altitude. This adverse gradient can preclude laminar flow aft of this region. However, it was possible to obtain the desired pressure distribution by performing a pushover maneuver, described in detail in reference 12.

An undesirable characteristic of the off-design pressure distribution at $M = 0.79$ is the shock that occurred near 50-percent chord. With glove 2 attached to the right wing, there was an extreme amount of Mach buffet at $M = 0.80$ and above because of this shock. The Mach buffet was noted at all sweep angles and was most severe at 20° of sweep. The Mach buffet limited the amount of data obtained at $M = 0.80$ and above, therefore the data was limited to $M = 0.79$. Despite the occurrence of the shock at approximately 50-percent chord, the relatively steep favorable gradient proved desirable for maintaining laminar flow at certain conditions, as discussed in the following section.

Boundary-Layer Transition Data

Figure 9(a) presents boundary-layer transition location (determined by hot films) $(x/c)_T$, plotted as a function of angle of attack for $\Lambda = 20°$, $M = 0.70$, and $hp = 35{,}000$ ft, at all test sections. The onset of the adverse gradient (AG) is plotted in figure 9(a) for all three test sections, in addition to the transition data. Figures 9(b), (c), and (d) show pressure distributions corresponding to each test section at three angles of attack, for the same flight condition.

The pressure distributions at this flight condition at the two lower angles of attack, $\alpha = 0.8$ and 1.7° (figs. 9(b) and (c)), have very mild, favorable pressure gradients. The AG begins at approximately 0.35 to 0.45 x/c at all three rows, presumably causing transition. However, for the middle and outboard stations, transition occurs as much as 0.15 x/c aft of the AG at angles of attack below 2.5° (fig. 9(a)). This is typical of the low-sweep data ($\Lambda \leq 25°$) obtained at conditions with mildly favorable or almost flat pressure gradients ($M \leq 0.70$), indicating that laminar flow can be maintained aft of the onset of an adverse gradient if the pressure gradients near the transition location are mild.

At conditions resulting in pressure distributions similar to those in figures 9(b) and (c), transition is believed to be caused by the loss of a favorable pressure gradient. This indicates that laminar flow may be maintained further aft along the chord, if the wing pressure distribution could be designed with the AG moved further aft.

At the outboard station of figure 9(a), transition occurs as much as 0.37 x/c aft of the AG for $\alpha > 2.5°$. The pressure distribution in figure 9(d), at $\alpha = 3.6°$, is an example of a pressure distribution at this condition. There is a peak near the leading edge in the glove pressure distributions, similar to that of figure 8 ($hp = 35{,}000$ ft, $M = 0.70$,

$\alpha = 3.0°$). In the pressure distribution for the outboard station, the peak occurs at 0.08 x/c. This leading-edge peak created a local area with an adverse gradient which did not cause transition.

This phenomena occurred at several test conditions. The steepness of the favorable gradient occurring ahead of the leading-edge peak appears to give the flow enough energy to remain laminar in the localized area of unfavorable pressure gradient.

Figure 10 presents boundary-layer transition data for $\Lambda_{eq} = 15°$, $M = 0.75$, and $hp = 35{,}000$ ft along with pressure distributions at three different angles of attack. In figure 10(a), transition occurs at 0.45 x/c or aft at all three stations, which is aft of the AG. The corresponding pressure distributions, figures 10(b) $\alpha = 0.6°$ and (c) $\alpha = 1.3°$, have a fairly steep favorable gradient at all three sections. At $\alpha = 3.4°$ (fig. 10(d)) the pressure gradient becomes flatter and a peak forms near 0.10 x/c, at the middle and outboard rows.

In this example, a steep favorable pressure distribution resulted in laminar flow to about 0.5 x/c at all three stations for the entire angle-of-attack range. However, the sweep was low, 15°. In most cases with low sweeps ($\Lambda < 25°$) and high Mach numbers ($M = 0.75, 0.80$), laminar flow was maintained to the AG or just aft. The steep favorable pressure gradient at $M = 0.75$ and above provided the optimum condition for maintaining laminar flow for sweeps below 25°. Transition is caused by the AG near 0.5 x/c.

Figure 11 presents transition data as a function of angle of attack, along with pressure distributions at three different angles of attack for $\Lambda = 25°$, $M = 0.70$, $hp = 20{,}000$ ft. In figure 11(a) transition occurs ahead of the AG in all cases, except for one point at the middle station. At sweep angles of 25° and above, transition usually occurred ahead of the AG as in this example. The corresponding pressure distributions (figs. 11(b), (c), and (d)) have favorable pressure gradients extending to approximately 0.4 x/c or aft at all angles of attack.

While all the pressure gradients between 0.1 and 0.4 x/c are mildly favorable, the steepest pressure gradient occurs at $\alpha = 0.0°$ (fig. 11(b)). As angle of attack increases, the pressure gradients flatten (figs. 11(c) and (d)). In figure 11(a), transition also moves aft with increasing angle of attack at all three stations. One reason for this is that the pressure gradient is flattening, apparently reducing the growth rate of the crossflow disturbances. The effect of pressure gradient on crossflow is discussed in reference 10.

Figure 12 shows transition data for $\Lambda = 25°$, $M = 0.70$, and $hp = 35{,}000$ ft. The unit Reynolds number for this case is approximately 1.7×10^6/ft; in the previous case the unit Reynolds number was approximately 2.9×10^6/ft. In figure 12(a) transition has moved aft, relative to figure 11(a), for all three stations. The inboard station transition location is still forward of the AG, but the majority of the data at the middle and outboard stations indicate that transition is occurring near or aft of the AG. The pressure distributions at the lower unit Reynolds number (figs. 12(b), (c), and (d)) have not changed significantly from those at the higher unit Reynolds number (figs. 11(b), (c), and (d)). This shows how a decrease in Reynolds number can have a favorable effect on transition.

Figure 13 presents transition data for $\Lambda = 35°$, $M = 0.70$, and $hp = 35{,}000$ ft. As figure 13(a) shows, the increased sweep has moved transition forward at all three stations, relative to the example of figure 12. The furthest aft transition locations, however, are occurring near the AG for the middle and outboard stations.

In figure 13(a), transition occurs near or aft of the AG for angles of attack greater than 1.8° for the middle and outboard stations. Transition occurs ahead of the AG for $\alpha < 2.0°$. The furthest aft transition location for the middle and outboard stations occurs at $\alpha = 1.8°$, 0.375 x/c, and 0.4 x/c respectively.

In comparing the pressure distribution at $\alpha = 0.7°$, figure 13(b) has a very mild favorable gradient up to 0.4 x/c or aft. At $\alpha = 1.8°$, where the furthest aft transition occurs (fig. 14(c)) the pressure gradients are flat, with a slight leading-edge peak at the outboard station. At $\alpha = 4.1°$ (fig. 14(d)) there is a leading-edge peak at all three stations. This sensitivity to the pressure gradient is typical of the transition data above 25° of sweep and indicates that a flat rather than a favorable pressure distribution may be the optimum for encouraging laminar flow, if the unit Reynolds number is not too high. One other possible explanation is the sensitivity of transition to the attachment line location.

Maximum Transition Location

Figures 14 through 18 present the maximum boundary-layer transition locations as a function of sweep for the inboard, middle and outboard sections at all test conditions. The maximum transition location was determined from the plots of transition location as a function of angle of attack obtained at each condition. Examples of these plots are shown in figures 9(a), 10(a), 11(a), 12(a), and 13(a).

Generally, the transition location moves forward with increasing sweep, as expected. At the furthest aft transition locations in most cases boundary-layer transition was caused by the AG, especially at sweeps of 25° and below. Also, at sweeps of 15 and 20°, transition occurred at 55-percent chord, which is at the aft edge of the glove, for many test conditions. Therefore, obtaining more laminar flow at these conditions may be possible if a wing could be designed to have an airfoil shape that provided a favorable pressure gradient extending further aft than those of glove 2. In addition, glove 2 was designed for 20° of sweep. More laminar flow may therefore be obtained at higher sweeps using a wing designed specifically for higher sweeps.

Maximum Transition Reynolds Number

The maximum transition Reynolds numbers obtained are shown in figure 19 as a function of sweep for several Mach numbers and are tabulated in table 9. As the wing sweep increases, the transition Reynolds numbers generally decrease for all Mach numbers. The highest transition Reynolds number obtained was 18.6×10^6, occurring at an equivalent sweep of 15°, $M = 0.75$, and an altitude of 10,000 ft. This is onc of the highest transition Reynolds numbers recorded for an NLF experiment.

At the lower sweep angles ($\Lambda < 25°$), the maximum transition Reynolds numbers usually occurred at 10,000 and 20,000 ft, higher unit Reynolds number conditions. At sweeps above 25°, the maximum transition Reynolds numbers, in all cases but one, occurred at 30,000 and 35,000 ft, lower unit Reynolds number conditions.

Momentum Thickness

Momentum thickness (θ) is an indicator of the viscous losses in the boundary layer. Figure 20 presents momentum thickness as a function of transition location at $M = 0.70$ and $\Lambda = 20°$. These data were obtained during the glove 2 boundary-layer rake calibration flights, conducted using the forced transition method discussed in reference 14. Table 7 contains the tabulated boundary-layer data used to obtain the results presented in figure 20. The tabulated data is provided for further boundary-layer analysis. Significantly, momentum thickness is reduced by more than 50 percent when transition is delayed from 10-percent chord to 50-percent chord. Such a reduction in momentum thickness resulting in moving the transition location aft is directly translatable to a reduction in skin friction drag on a transport or a business jet.

Two qualifying statements apply to the viscous drag reduction data presented. First, this experiment was not a complete airfoil test; only the forward 60-percent portion of the upper wing surface was gloved. These results indicate an optimum reduction on the upper surface only. Second, these results were not obtained at trimmed lift coefficients; a pushover or level-turn maneuver was required to attain some of the conditions that provide laminar flow. However, there is no reason to expect that an airfoil contoured specifically for the optimum angle of attack could not attain comparable amounts of laminar flow at working, or cruise lift coefficients.

CONCLUDING REMARKS

This report presents the results and discussions on the boundary-layer transition data obtained for glove 2 of the variable-sweep transition flight experiment. Transition location was determined as a function of wing sweep with

respect to pressure distribution, Reynolds number, Mach number, and angle of attack. The transition data presented were obtained from hot-film sensors, with a limited amount of data obtained from boundary-layer rakes.

The transition database established includes leading-edge sweeps of 15 to 35°, Mach numbers ranging from 0.60 to 0.79, and altitudes ranging from 10,000 to 35,000 ft. The following trends were noted in the data.

The maximum transition Reynolds number, 18.6×10^6, occurred at an equivalent sweep of 15°, a Mach number of 0.75, and an altitude of 10,000 ft. This is believed to be one of the highest natural boundary-layer transition Reynolds numbers on record.

A steep favorable pressure gradient, typical for $M = 0.75$ and above, provided the optimum condition for maintaining laminar flow at wing sweeps below 25°. It did not, however, result in an appreciable amount of laminar flow for 30 and 35° of sweep.

At wing sweeps above 25°, the transition location was highly sensitive to the pressure gradient. The transition data indicates that a flat, rather than a mildly favorable pressure distribution may be the optimum for encouraging laminar flow at sweeps above 25°.

At 35° of sweep, 35,000 ft, and $M = 0.70$, laminar flow could be maintained to the AG (~40-percent chord) for the optimum angle of attack range. Based on the transition data obtained, laminar flow could be maintained further downstream if the airfoil was tailored for the desired sweep.

The transition results obtained at sweeps below 25° and Mach numbers below 0.70 indicate that laminar flow can be maintained aft of the AG if the pressure gradients are mild near the transition location.

REFERENCES

1. Boeing Commercial Airplane Company, *Natural Laminar Flow Airfoil Analysis and Studies*, NASA CR-159029, 1979.

2. Boeing Commercial Airplane Company, *Evaluation of Laminar Flow Control System Concepts for Subsonic Commercial Transport Aircraft*, NASA CR-158796, 1978.

3. Lockheed-Georgia Company, *Evaluation of Laminar Flow Control System Concepts for Subsonic Commercial Transport Aircraft*, NASA CR-159253, 1980.

4. McDonnell Douglas Corporation, *Evaluation of Laminar Flow Control System Concepts for Subsonic Commercial Transport Aircraft*, NASA CR-159251, 1983.

5. Wagner, R.D., and M.C. Fischer, "Developments in the NASA Transport Aircraft Laminar Flow Program," AIAA-83-0090, Jan. 1983.

6. Montoya, L.C., L.L. Steers, D.C. Christopher, and B.M. Trujillo, *F-111 TACT Natural Laminar Flow Glove Flight Results*, NASA CP-2208, 1981.

7. Meyer, Robert R., Jr., and Lisa A. Jennett, *In-Flight Surface Oil-Flow Photographs With Comparisons to Pressure Distribution and Boundary-Layer Data*, NASA TP-2395, 1985.

8. Boeing Commercial Airplane Company, *F-111 Natural Laminar Flow Glove Flight Test Data Analysis and Boundary Layer Stability Analysis*, NASA CR-166051, 1984.

9. Waggoner, E.G., P.S. Phillips, J.K. Viken, and W.H. Davis, "Potential Flow Calculations and Preliminary Wing Design in Support of an NLF Variable-Sweep Transition Flight Experiment," AIAA 85-0426, Jan. 1985.

10. Waggoner, E.G., R.L. Campbell, P.S. Phillips, and J.B. Hallissy, *Design and Tests of an NLF Wing Glove for the Variable-Sweep Transition Flight Experiment*, NLF and LFC Research Symposium, Langley Research Center, Hampton, VA, Mar. 16–19, 1987, NASA CP-2487, Part 3, pp. 753–776.

11. Rozendaal, Rodger A., *Variable-Sweep Transition Flight Experiment (VSTFE) - Parametric Pressure Distribution Boundary-Layer Stability Study and Wing Glove Design Task*, NASA CR-3992, 1986.

12. Meyer, Robert R., Bianca M. Trujillo, and Dennis W. Bartlett, *F-14 VSTFE and Results of the Cleanup Flight Test Program*, NLF and LFC Research Symposium, Langley Research Center, Hampton, VA, Mar. 16–19, 1987, NASA CP-2487, Part 3, pp. 819–844.

13. Rozendaal, Rodger A., *Variable-Sweep Transition Flight Experiment (VSTFE) - Stability Code Development and Clean-Up Glove Data Analysis*, NLF and LFC Research Symposium, Langley Research Center, Hampton, VA, Mar. 16–19, 1987, NASA CP-2487, Part 2, pp. 845–860.

14. Anderson, Bianca Trujillo, Robert R. Meyer, Jr., and Harry R. Chiles, "Techniques Used in the F-14 Variable-Sweep Transition Flight Experiment," AIAA-88-2110, May 1988.

15. Anderson, Bianca Trujillo, and Robert R. Meyer, Jr., *Effects of Wing Sweep on Boundary-Layer Transition for a Smooth F-14A Wing at Mach Numbers From 0.700 To 0.825*, NASA TM-101712, 1990.

16. Bohn-Meyer, M., and Fred Jiran, "The Use of Techniques to Modify Airfoils and Fairings on Aircraft Using Foam and Fiberglass," AIAA-81-2445, Nov. 1981.

17. Bohn-Meyer, Marta M., "Constructing 'Gloved' Wings for Aerodynamic Studies," AIAA-88-2109, May 1988.

18. Chiles, Harry R., *The Design and Use of a Temperature Compensated Hot-Film Anemometer System For Boundary-layer Flow Transition Detection on Supersonic Aircraft*, NASA TM-100421, 1988.

19. DeAnda, Albert G., *AFFTC Standard Airspeed Calibration Procedures*, AFFTC-TIH-81-5, June 1981.

20. Johnson, J. Blair, Terry J. Larson, and Jules M. Ficke, *Digital Program for Calculating Static Pressure Position Error*, NASA TM-86726, 1987.

21. Sakamoto, G.M., *Aerodynamic Characteristics of a Vane Flow Angularity Sensor System Capable of Measuring Flight Path Accelerations for the Mach Number Range from 0.4 to 2.54*, NASA TN D-8242, 1976.

22. Davis, Richard E., Dal V. Maddalon, Richard D. Wagner, David F. Fisher, and Ronald Young, *Evaluation of Cloud Detection Instruments and Performance of Laminar-Flow Leading-Edge Test Articles During NASA Leading-Edge Flight-Test Program*, NASA TP-2888, 1989.

23. Meyer, R.R., Jr., and Cdr. E.T. Schneider, "Real-Time Pilot Guidance System for Improved Flight Test Maneuvers," AIAA-83-2747, Nov. 1983.

Table 1. Glove 2 airfoil coordinates.

	y/c			
x/c	BL 130	BL 200	BL 274	BL 348
0.00000	−0.009173	0.005030	−0.002880	−0.021320
0.00191	−0.004751	0.009250	0.001060	−0.014980
0.00496	−0.000419	0.013260	0.004290	−0.010330
0.00995	0.004891	0.017810	0.008390	−0.005480
0.02000	0.012905	0.024250	0.014640	0.001170
0.03993	0.024105	0.032820	0.023760	0.010010
0.06000	0.032545	0.038970	0.030440	0.016790
0.08000	0.039329	0.043910	0.035880	0.022510
0.10000	0.044944	0.048090	0.040360	0.027520
0.12000	0.049724	0.051960	0.044330	0.032000
0.14000	0.053866	0.054840	0.047840	0.036030
0.16000	0.057500	0.057630	0.050980	0.039710
0.18000	0.060690	0.060090	0.053780	0.043090
0.20000	0.063511	0.062270	0.056290	0.046230
0.22000	0.065969	0.064190	0.058550	0.049130
0.24000	0.068125	0.065860	0.060560	0.051820
0.26000	0.069972	0.067300	0.062330	0.054290
0.28000	0.071538	0.068520	0.063860	0.056560
0.30000	0.072826	0.069510	0.065170	0.058620
0.32000	0.073843	0.070270	0.066240	0.060480
0.34000	0.074582	0.070810	0.067100	0.062140
0.36000	0.075052	0.071120	0.067720	0.063580
0.38000	0.075243	0.071220	0.068120	0.064820
0.40000	0.075126	0.071080	0.068290	0.065840
0.42000	0.074737	0.070690	0.068200	0.066630
0.44000	0.074010	0.070060	0.067860	0.067180
0.46000	0.072894	0.069170	0.067260	0.067470
0.48000	0.071408	0.068010	0.066390	0.067500
0.50000	0.069474	0.066580	0.065260	0.067250
0.52000	0.067098	0.064870	0.063890	0.066710
0.56000	0.061281	0.060600	0.060500	0.064810
0.60000	0.054750	0.055190	0.056350	0.061890

Table 2. Surface pressure orifice locations.

Location	BL station, in.	Chord, in.	Chord, percent
Row 1	140.0	126.4	
Row 2	200.8	103.7	
Row 3	260.0	84.8	
Row 4	320.0	65.4	
Upper surface			0.0, 0.15, 0.3, 0.5, 1.0, 2.0, 4.0, 6.0, 8.0, 10.0, 12.0, 15.0, 17.0, 20.0, 25.0, 30.0, 35.0, 40.0, 45.0, 50.0, 55.0
Lower surface			0.15, 0.3, 0.5, 1.0

Table 3. Boundary-layer rake locations.

Locations	Rake 1	Rake 2
BL station, in.	230	290
Chord, percent	55.0	55.0
Nominal rake probe heights, in.	0.05	0.05
	0.07	0.07
	0.13	0.13
	0.17	0.18
	0.22	0.23
	0.27	0.27
	0.33	0.32
	0.39	0.38
	0.43	0.42
	0.53	0.53
	0.73	0.73
	0.94	0.93
	1.13	1.13
	1.34	1.35
	1.54	1.54
	1.75	1.74
	1.94	1.95
	2.16	2.15
	2.37	2.35
	2.60	2.58

Table 4. Hot-film anemometer locations.

Flight	Station 1, (BL 162–196), percent chord	Station 2, (BL 228–256), percent chord	Station 3, (BL 294–316), percent chord
36–45	10, 20, 30, 40, 50	10, 20, 30, 40, 50	10, 20, 30, 40, 50
46–49	30, 35, 40, 45, 50	30, 35, 40, 45, 50	30, 35, 40, 45, 50
50–52	5, 10, 15, 20, 25	5, 10, 15, 20, 25	5, 10, 15, 20, 25
53–68	10, 20, 30, 40, 50	10, 20, 30, 40, 50	10, 20, 30, 40, 50
53–57, 59–61	Natural transition	Forced transition	Forced transition

Table 5. Flight test conditions.

Mach	hp, ft	α, deg
0.60	10,000	0.0 – 3.2
	20,000	0.0 – 3.1
	25,000	0.5 – 4.3
	30,000	– – –
	35,000	3.5 – 4.1
0.65	10,000	−0.3 – 2.3
	20,000	0.0 – 2.4
	25,000	– – –
	30,000	0.5 – 4.3
	35,000	0.0 – 6.0
0.70	10,000	−0.4 – 2.0
	20,000	0.0 – 3.1
	25,000	0.5 – 5.7
	30,000	0.3 – 3.9
	35,000	0.0 – 5.2
0.75	10,000	−0.4 – 1.1
	20,000	−0.4 – 3.0
	25,000	0.0 – 3.1
	30,000	0.0 – 3.6
	35,000	0.0 – 3.9
0.79	10,000	−0.6 – 1.0
	20,000	−0.4 – 2.4
	25,000	0.0 – 2.2
	30,000	2.5
	35,000	1.0 – 3.3

Table 6. Glove section pressure coefficients.
Microfiche pages m-1 through m-1583.

Table 7. Boundary-layer velocity profile data.
Microfiche pages m-1584 through m-2809.

Table 8. Boundary-layer transition locations.
Microfiche pages m-2810 through m-2844.

Tables 6–8 are in the microfiche supplement included with this report and are also available on disk from the author on request.

Table 9. Maximum transition Reynolds number for each wing sweep.

Sweep, deg	$Re_T \times 10^6$	Mach	hp, ft
15 - inboard	12.80	0.75	20,600
15 - middle	18.62	0.75	11,400
15 - outboard	12.16	0.65	10,000
20 - inboard	8.93	0.70	30,000
20 - middle	14.29	0.75	20,100
20 - outboard	10.03	0.75	20,000
25 - inboard	6.32	0.70	29,900
25 - middle	12.12	0.75	20,800
25 - outboard	8.40	0.75	20,800
30 - inboard	4.10	0.75	35,200
30 - middle	5.93	0.70	35,100
30 - outboard	5.57	0.60	20,000
35 - inboard	2.70	0.65	29,900
35 - middle	4.89	0.70	34,900
35 - outboard	4.35	0.70	29.500

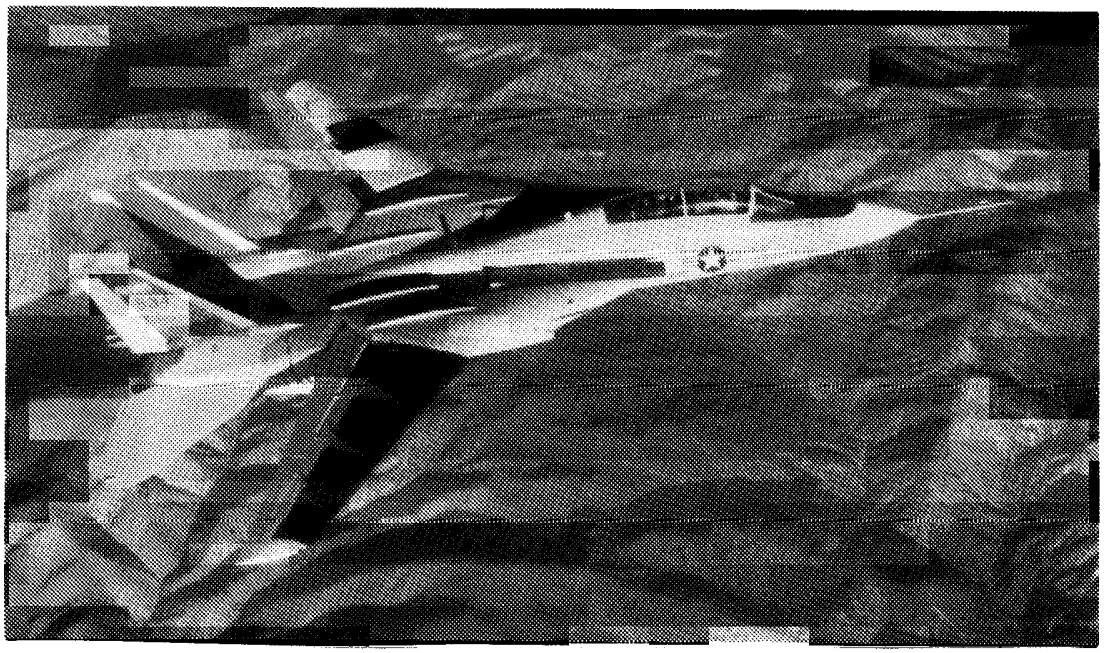

EC87 0100-018

Figure 1. The F-14A aircraft with glove 1 on the left wing and glove 2 on the right wing.

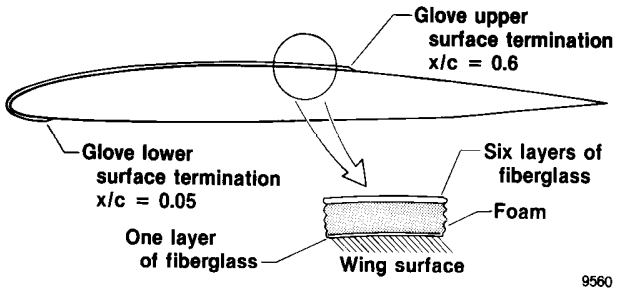

Figure 2. Glove 2 typical cross section.

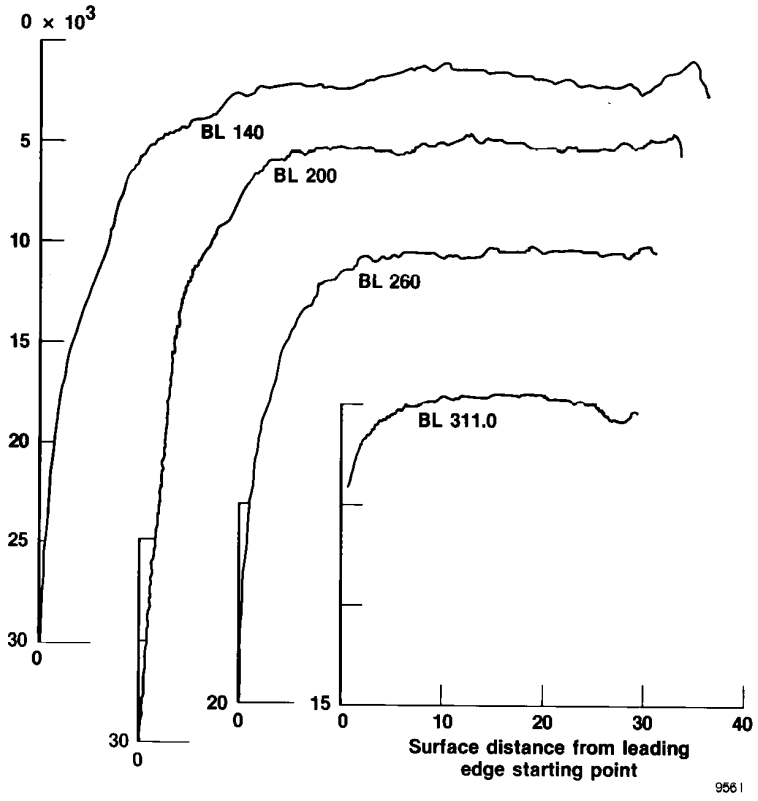

(a) Waviness measurements.

Figure 3. Glove 2 waviness.

EC85 32574

(b) Mechanical deflection dial gauge.

Figure 3. Concluded.

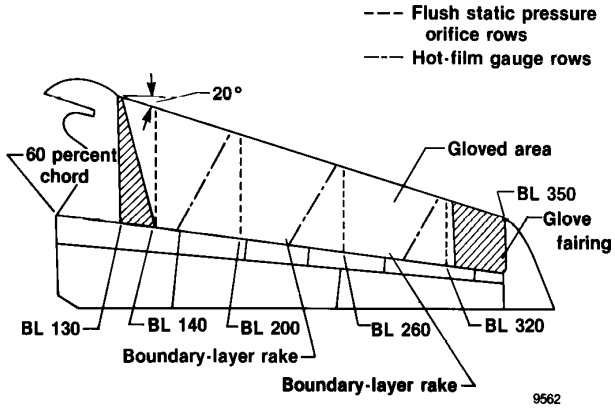

Figure 4. Glove 2 instrumentation layout.

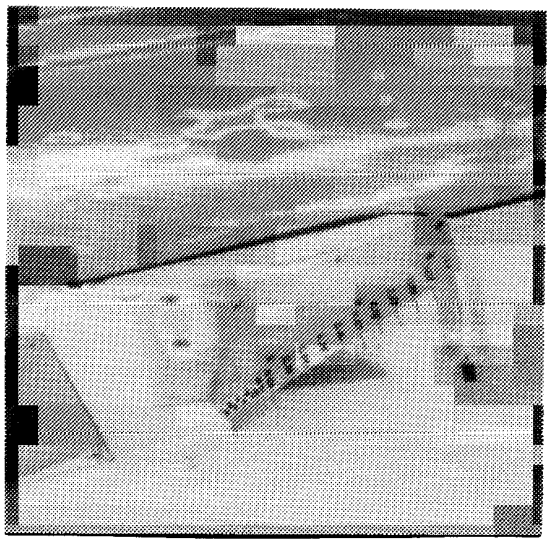

EC 33404-004

Figure 5. Boundary-layer rake.

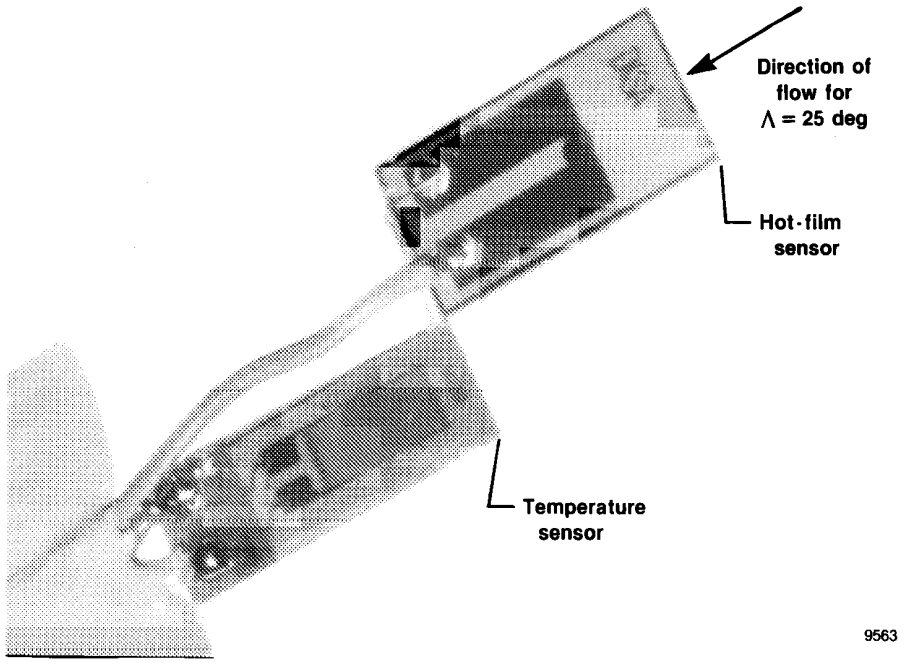

Figure 6. Temperature compensated hot-film sensor.

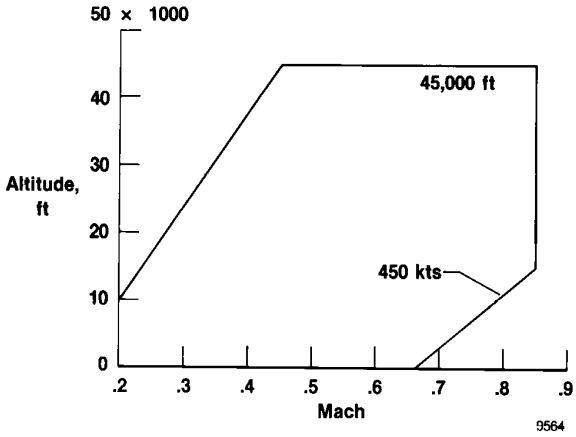

Figure 7. Glove 2 operating envelope.

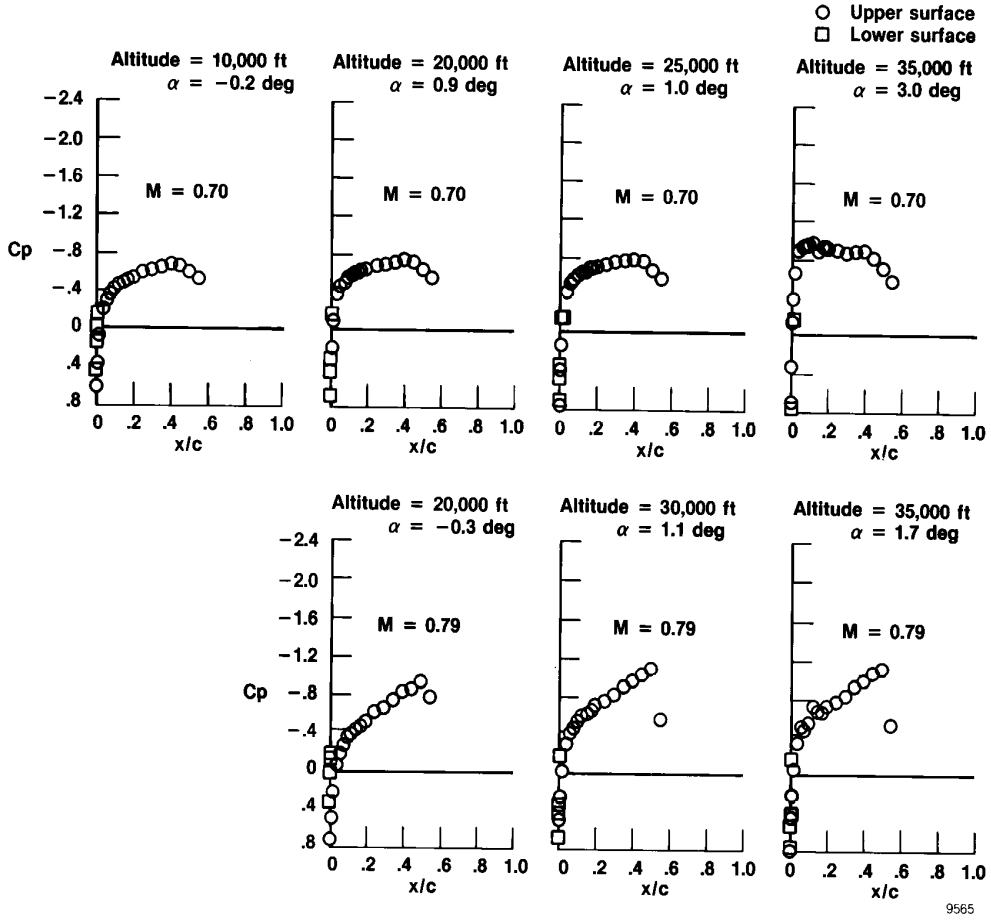

Figure 8. Glove 2 pressure distribution at trim angles of attack for middle station, $\Lambda = 20°$.

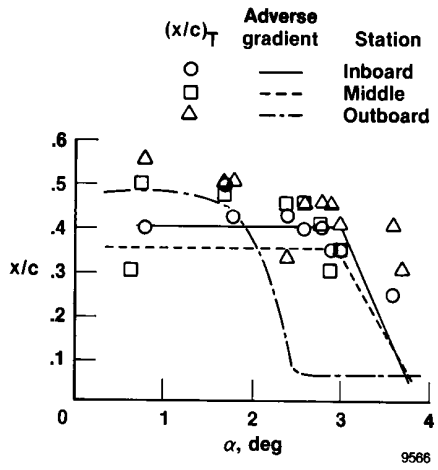

(a) Boundary-layer transition location and onset of AG.

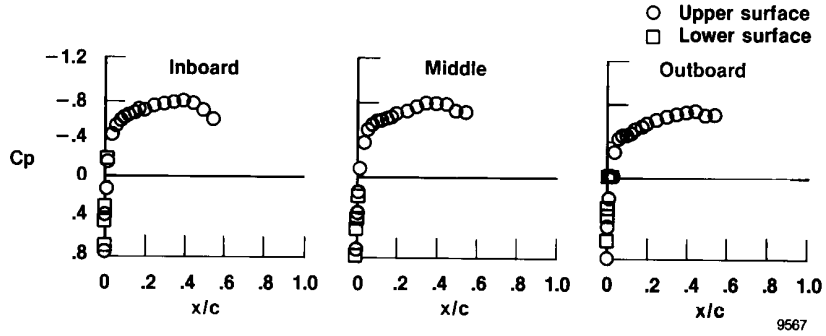

(b) Pressure distribution, $\alpha = 0.80°$.

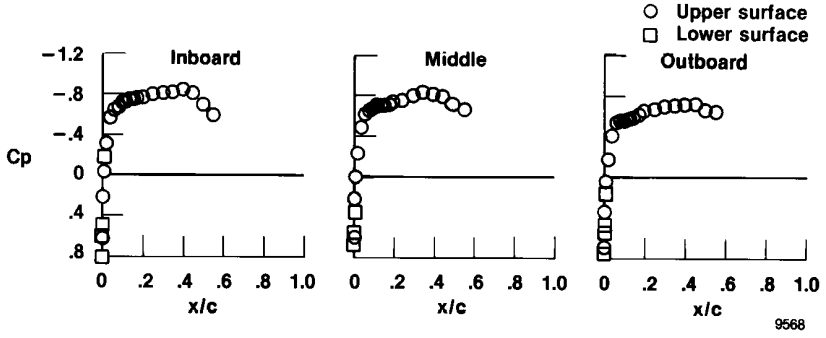

(c) Pressure distribution, $\alpha = 1.7°$.

Figure 9. Transition data and pressure distributions for $\Lambda = 20°$, $M = 0.70$, and $hp = 35{,}000$ ft.

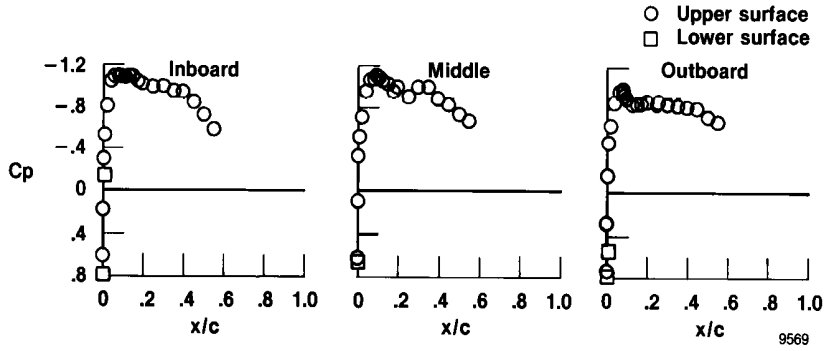

(d) Pressure distributions, $\alpha = 3.6°$.

Figure 9. Concluded.

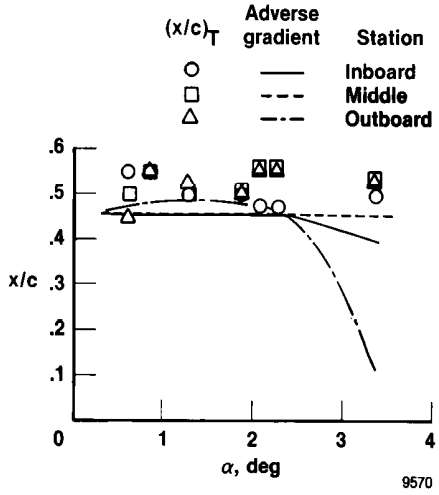

(a) Boundary-layer transition location and onset of AG.

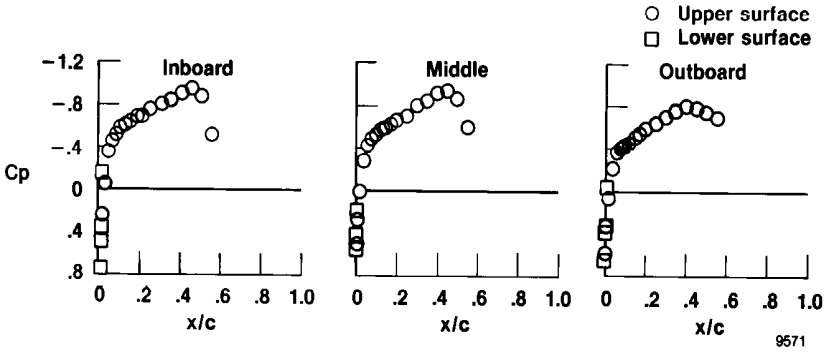

(b) Pressure distribution, $\alpha = 0.60°$.

Figure 10. Transition data and pressure distributions for $\Lambda_{eq} = 15°$, $M = 0.70$, and $hp = 35{,}000$ ft.

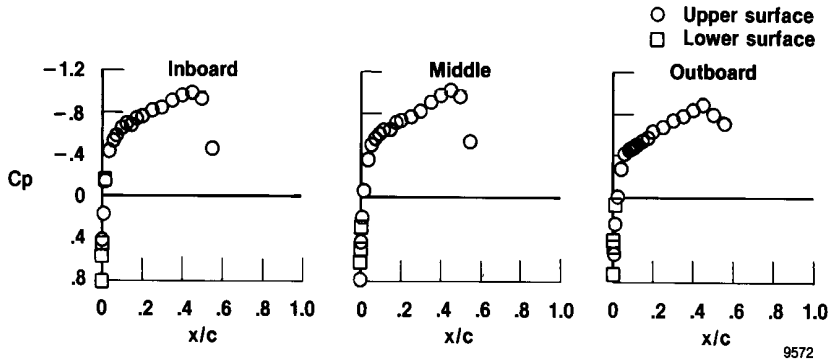

(c) Pressure distribution, $\alpha = 1.3°$.

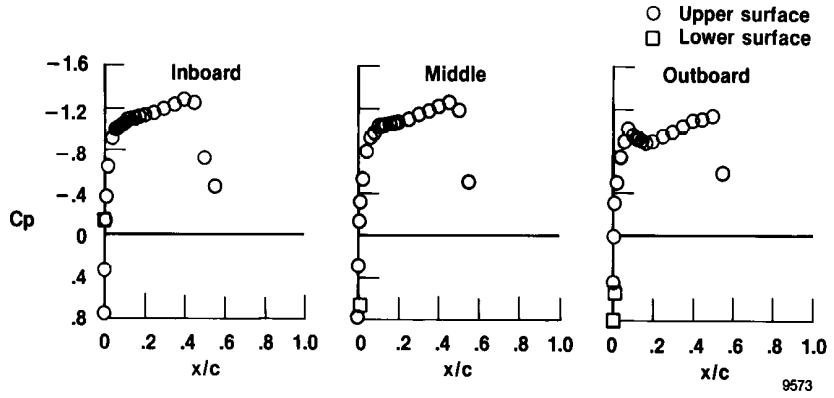

(d) Pressure distribution, $\alpha = 3.4°$.

Figure 10. Concluded.

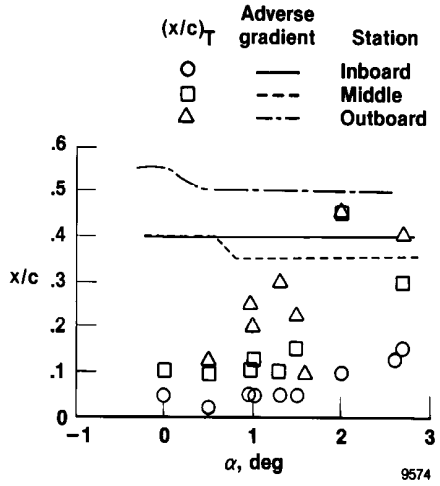

(a) Boundary-layer transition location and onset of AG.

Figure 11. Transition data and pressure distributions for $\Lambda = 25°$, $M = 0.70$, and $hp = 20{,}000$ ft.

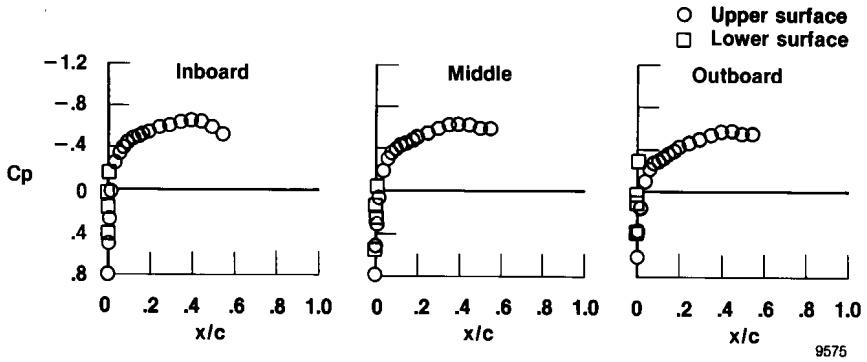

(b) Pressure distribution, $\alpha = 0.0°$.

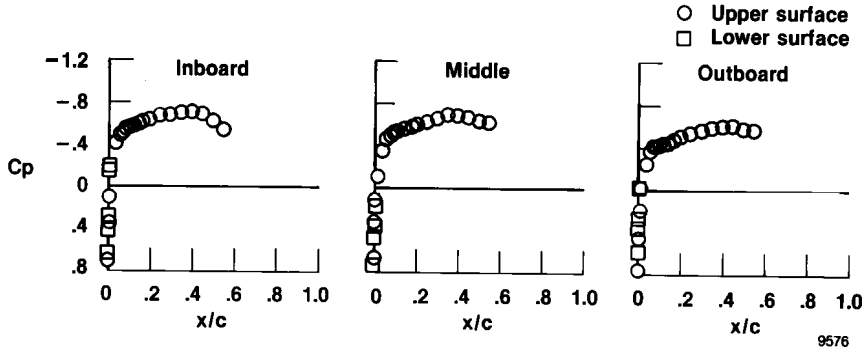

(c) Pressure distribution, $\alpha = 1.0°$.

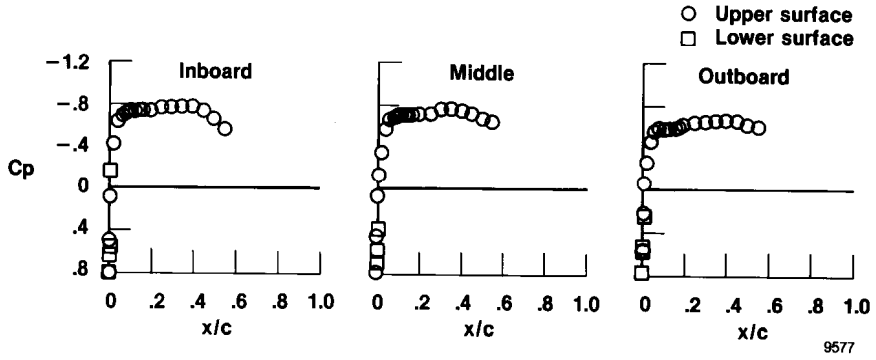

(d) Pressure distribution, $\alpha = 2.0°$.

Figure 11. Concluded.

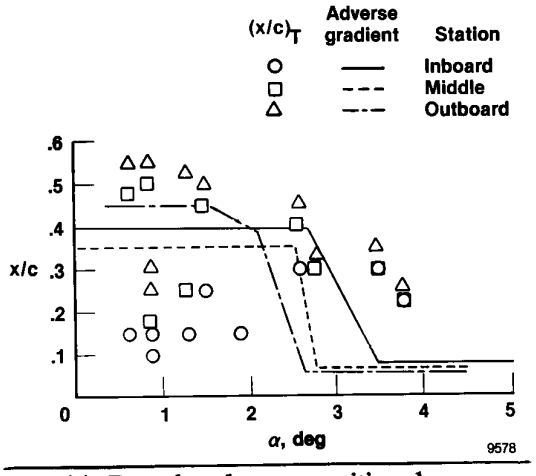

(a) Boundary-layer transition location and onset of AG.

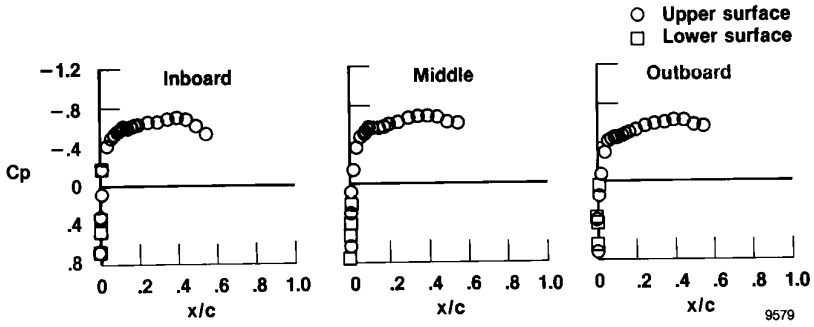

(b) Pressure distribution, $\alpha = 0.9°$.

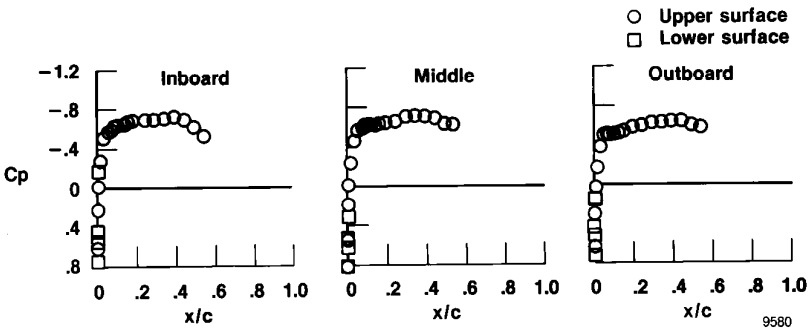

(c) Pressure distribution, $\alpha = 1.5°$.

Figure 12. Transition data and pressure distributions for $\Lambda = 25°$, $M = 0.70$, and $hp = 35{,}000$ ft.

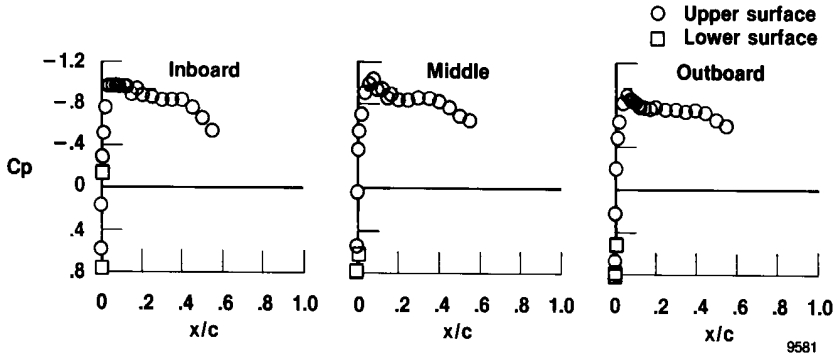

(d) Pressure distribution, $\alpha = 3.5°$.

Figure 12. Concluded.

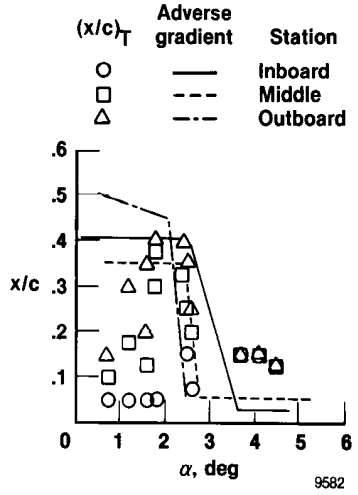

(a) Boundary-layer transition location and onset of AG.

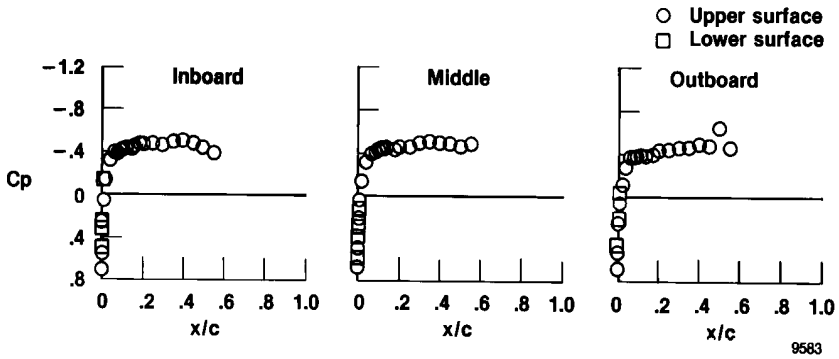

(b) Pressure distribution, $\alpha = 0.7°$.

Figure 13. Transition data and pressure distributions for $\Lambda = 35°$, $M = 0.70$, and $hp = 35{,}000$ ft.

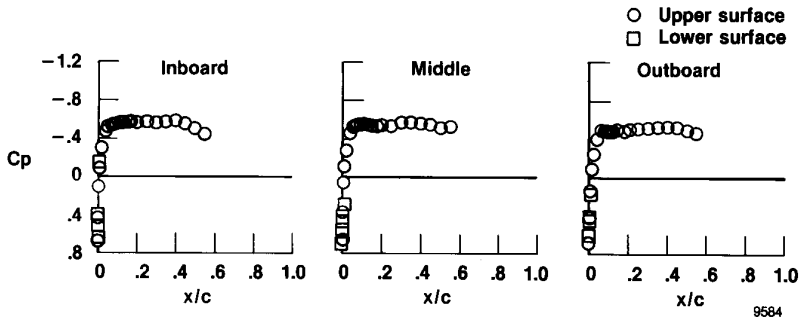

(c) Pressure distribution, $\alpha = 1.8°$.

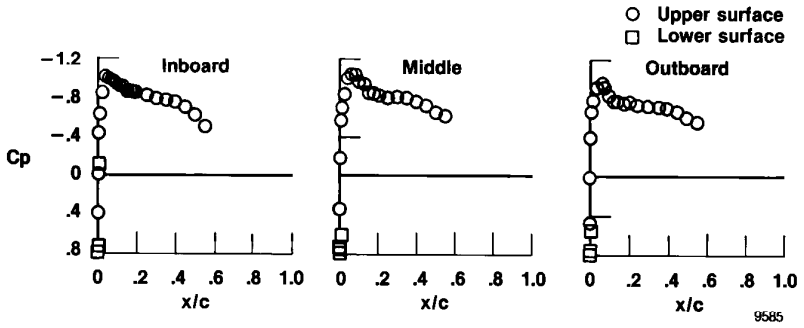

(d) Pressure distribution, $\alpha = 4.1°$.

Figure 13. Concluded.

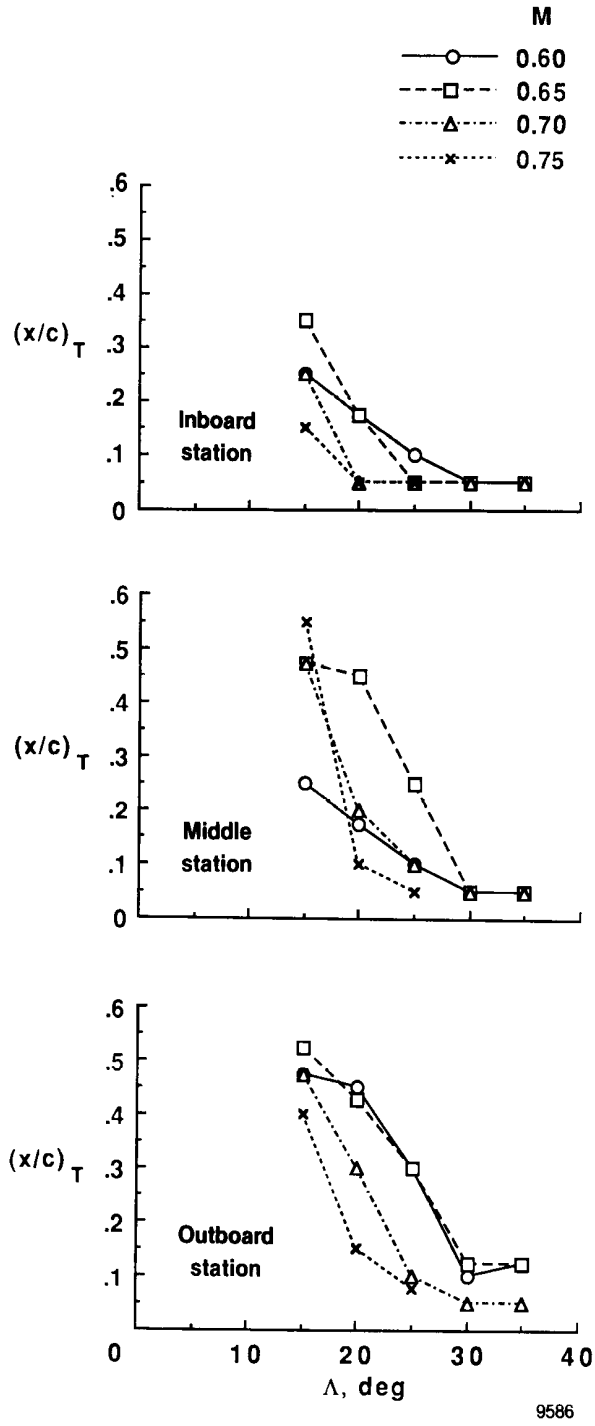

Figure 14. Maximum transition location as a function of sweep, hp = 10,000 ft.

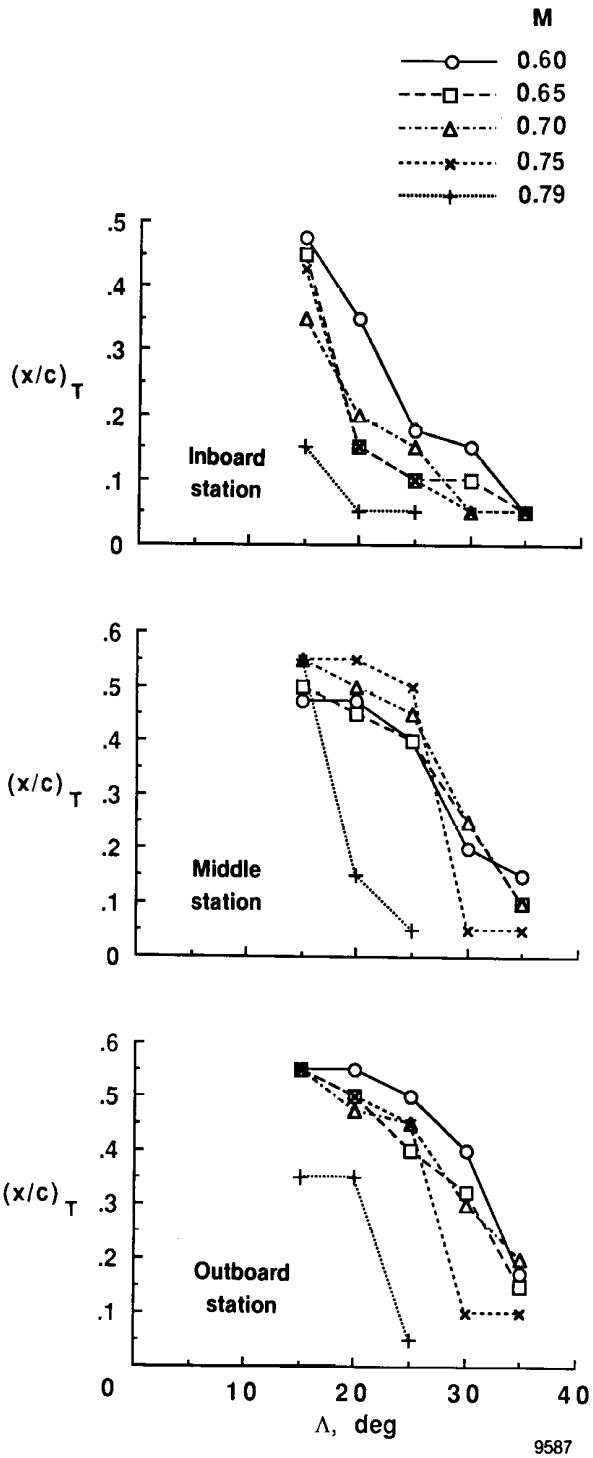

Figure 15. Maximum transition location as a function of sweep, hp = 20,000 ft.

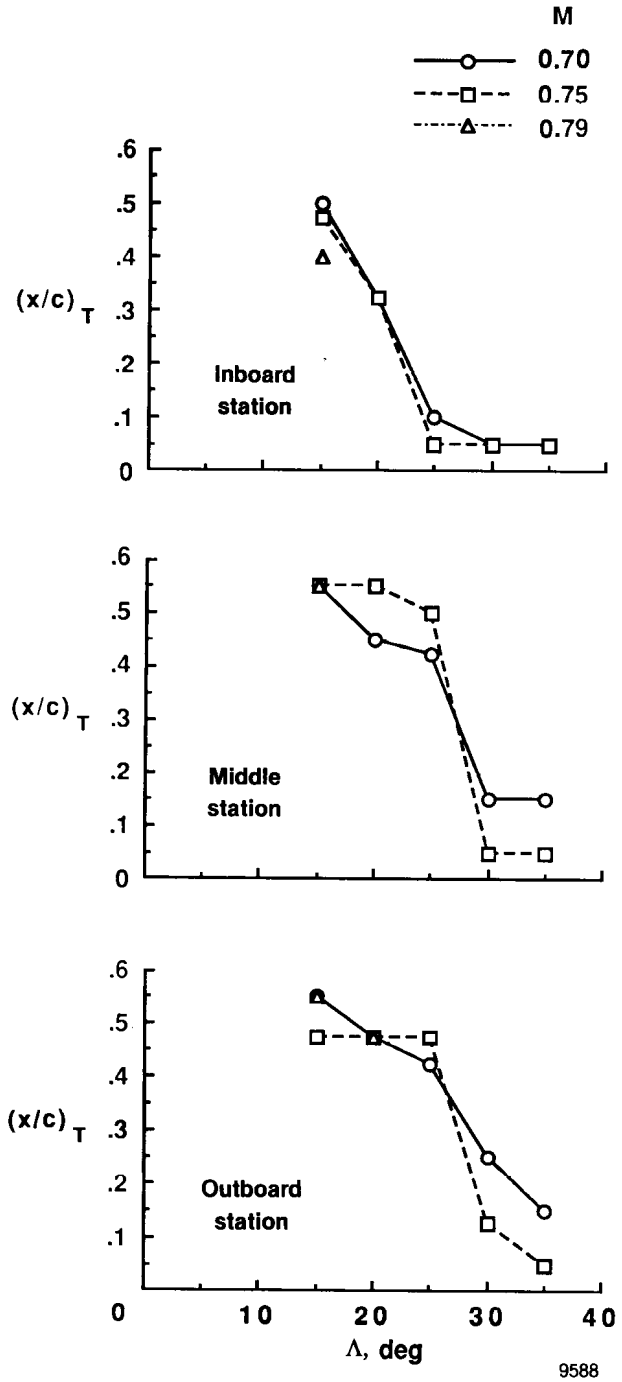

Figure 16. Maximum transition location as a function of sweep, hp = 25,000 ft.

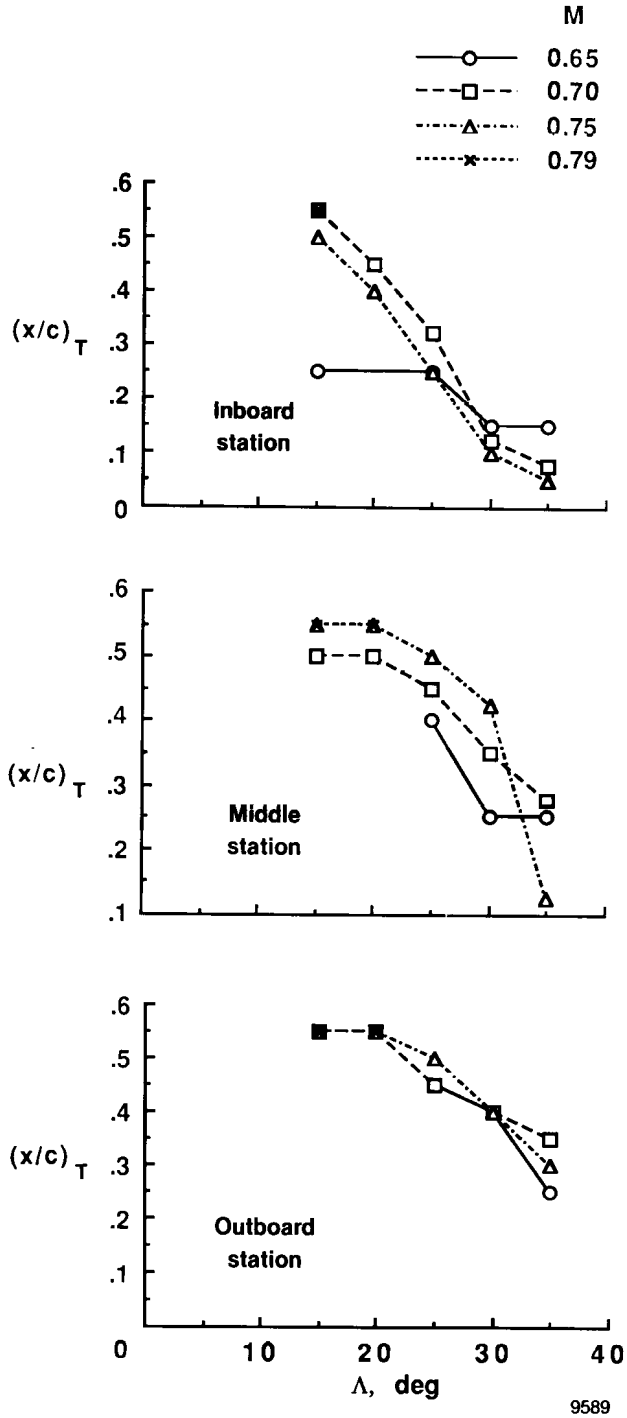

Figure 17. Maximum transition location as a function of sweep, hp = 30,000 ft.

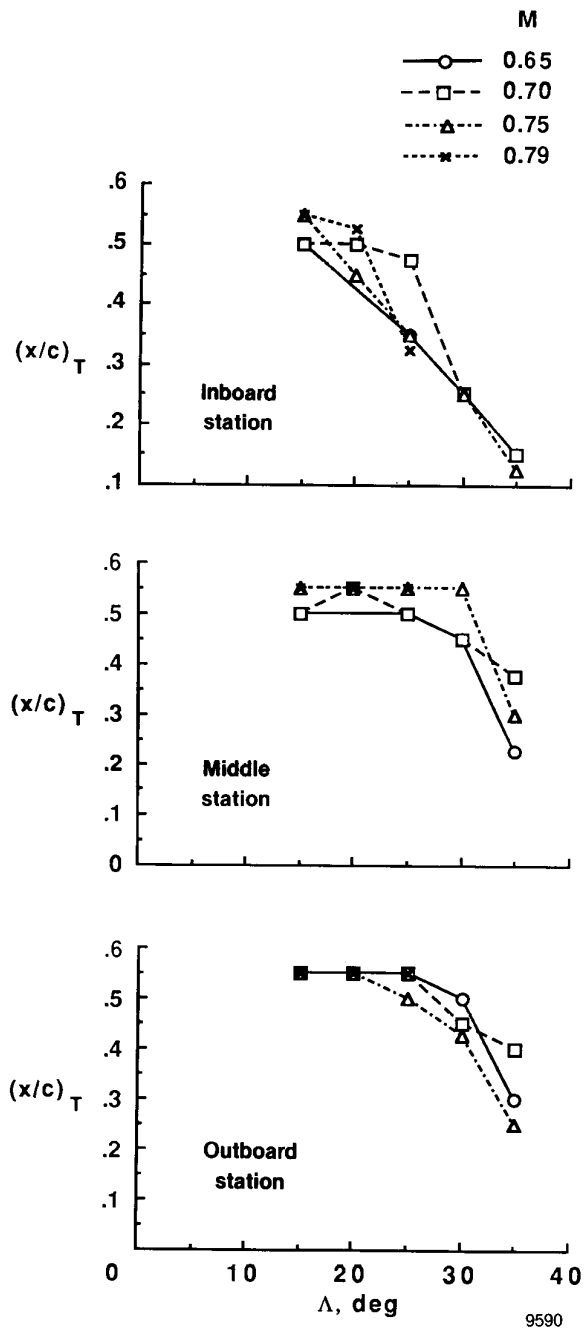

Figure 18. Maximum transition location as a function of sweep, hp = 35,000 ft.

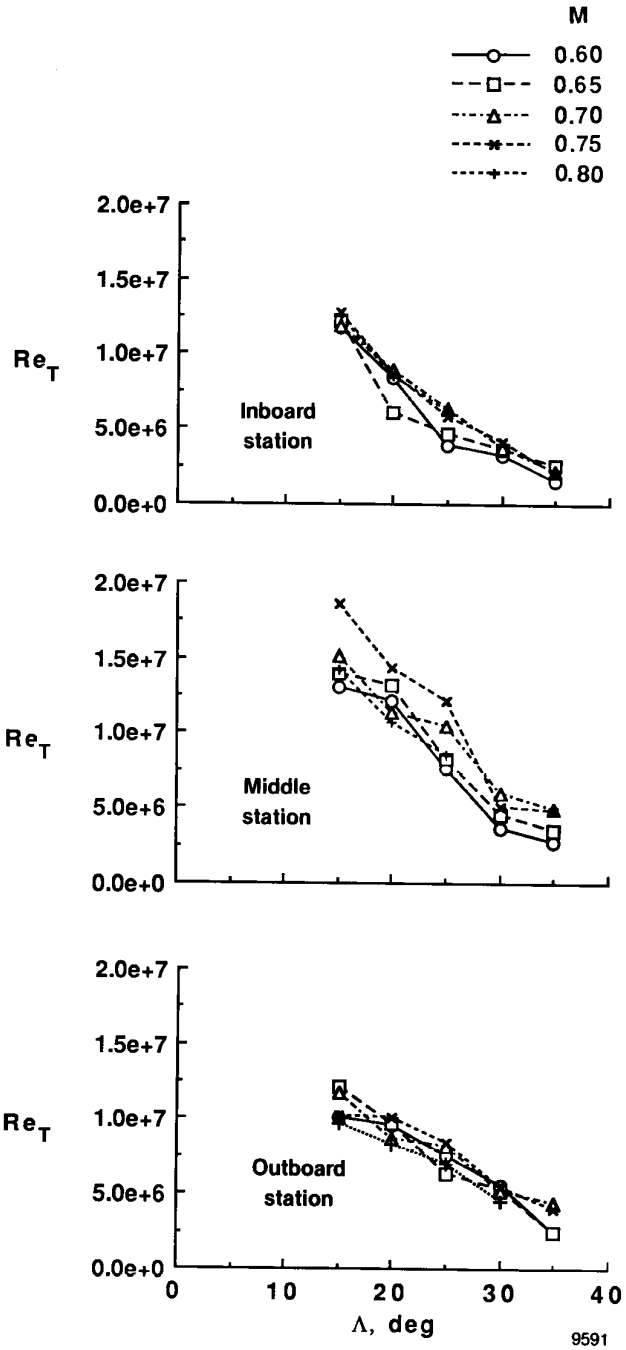

Figure 19. Maximum transition Reynolds number as a function of sweep.

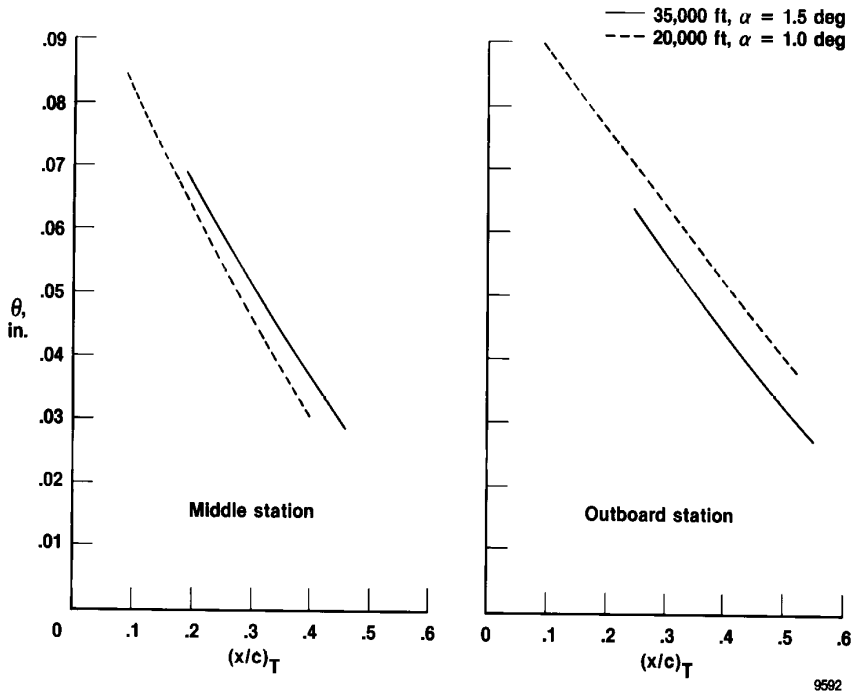

Figure 20. Momentum thickness as a function of transition location for $M = 0.70$, $\Lambda = 20°$.

NASA
National Aeronautics and Space Administration

Report Documentation Page

1. Report No.	2. Government Accession No.	3. Recipient's Catalog No.
NASA TM-101701		

4. Title and Subtitle

Effects of Wing Sweep on In-Flight Boundary-Layer Transition for a Laminar Flow Wing at Mach Numbers From 0.60 to 0.79

5. Report Date
July 1990

6. Performing Organization Code

7. Author(s)

Bianca Trujillo Anderson and Robert R. Meyer, Jr.

8. Performing Organization Report No.
H-1565

10. Work Unit No.
RTOP 505-60-4X

9. Performing Organization Name and Address

NASA Ames Research Center
Dryden Flight Research Facility
P.O. Box 273, Edwards, California 93523-0273

11. Contract or Grant No.

13. Type of Report and Period Covered
Technical Memorandum

12. Sponsoring Agency Name and Address

National Aeronautics and Space Administration
Washington, DC 20546-0001

14. Sponsoring Agency Code

15. Supplementary Notes

This report includes a microfiche supplement attached inside the back cover.

16. Abstract

The variable-sweep transition flight experiment (VSTFE) was conducted on an F-14A variable-sweep wing fighter to examine the effect of wing sweep on natural boundary-layer transition. Nearly full span upper surface gloves, extending to 60-percent chord, were attached to the F-14 aircraft's wings. This report presents the results of the glove 2 flight tests. Glove 2 had an airfoil shape designed for natural laminar flow at a wing sweep of 20°. Sample pressure distributions and transition locations are presented with the complete results tabulated in a database. Data were obtained at wing sweeps of 15, 20, 25, 30, and 35°, at Mach numbers ranging from 0.60 to 0.79, and at altitudes ranging from 10,000 to 35,000 ft. Results show that a substantial amount of laminar flow was maintained at all the wing sweeps evaluated. The maximum transition Reynolds number obtained was 18.6×10^6 at 15° of wing sweep, Mach 0.75, and at an altitude of 10,000 ft.

17. Key Words (Suggested by Author(s))

Boundary-layer transition
Laminar flow
Natural laminar flow

18. Distribution Statement

FEDD

Subject Category 34

19. Security Classif. (of this report)	20. Security Classif. (of this page)	21. No. of Pages	22. Price
Unclassified	Unclassified	37	A03

NASA FORM 1626 OCT 86